URBAN AEROSOL BACKSCATTER PROPERTIES BASED ON RAMAN LIDAR AND PARAMETRIC COEFFICIENTS

J1.2

FOURTH SYMPOSIUM ON LIDAR ATMOSPHERIC APPLICATIONS

Daniela Viviana Vladutescu [1,2,*], Barry Gross[2], Yonghua Wu[2], Fred Moshary[2], Samir Ahmed[2]
1 New York City College of Technology (NYCCT/CUNY),
2 City College on the City University of New York (CCNY/CUNY)

1. INTRODUCTION

Human activities affect the global climate and may lead to large disturbances of the economic, social and political circumstances in the middle and long term. Understanding the dynamics of the Earth's climate is therefore of high importance and one of the major scientific challenges of our time. The estimation of the contribution of the Earth's climate system components needs observation and continuous monitoring of various atmospheric physical and chemical parameters. Temperature, water vapor and greenhouse gases concentration, aerosol and clouds loads, and atmospheric dynamics are parameters of particular importance in this respect. The quantification of the anthropogenic influence on the dynamics of these above-mentioned parameters is of crucial importance nowadays but still affected by significant uncertainties.

In the present context of these huge uncertainties in our understanding of how these different atmospheric compounds contribute to the climate processes, my paper presents the development of lidar (Light Detection and Ranging)-based remote sensing techniques for atmospheric monitoring and in particular the analyses of urban aerosol backscattering properties based on parametric coefficients and lidar measurements. These analyses exploit the aerosols hygroscopic properties and their interaction properties with light. The analyses presented here are based on the use the water vapor and aerosol backscatter measurements in the exploration of the nature and variability of urban aerosol hygroscopic properties using multi-wavelength Raman lidar measurements at 355nm, as well as backscatter measurements at 532nm and 1064nm. The addition of the longer wavelength channels allows us to more accurately validate the homogeneity of the aerosol layer as well as provide additional multi wavelength information that can be used to validate and modify the aerosol models underlying the hygroscopic trends observed in the Raman Channel.

The traditional method of investigation of the relationship between aerosol scattering and RH (relative humidity) was to use humidified nephelometer. However, at high RH this instruments are hard to control and **therefore alternative methods have been investigated. One of these methods is using lidar measurements (Phalow et al. (2006), Ferrare (1998)) for RH>85% to probe behavior of hygroscopic growth.**

2. MATHEMATICAL ANALYSIS

While it is difficult to model a realistic aerosol model requiring parameters which are laboratory based, we can explore a simplified model which is reasonable for the accumulation mode for aerosols. In particular, we assume general urban particle size distribution in conjunction with insitu measurements of sulfate, nitrate and organics concentrations collected in the proximity of the CCNY lidar system and more exactly at IS 52 in south Bronx, NY.

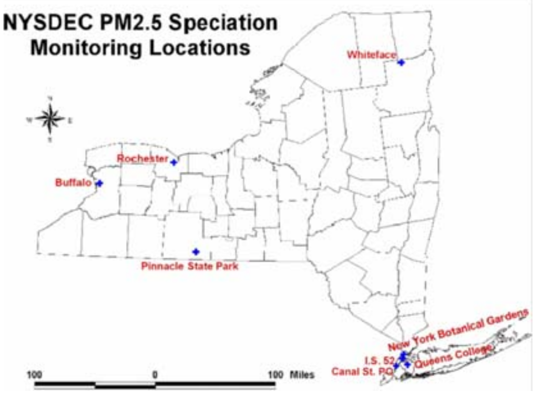

Figure1 NYSDEC Speciation Monitoring Locations

The number densjty of particles is calculated based on measured distribution on the east coast (Cabada et al, 2004). A representation of this distribution is given in figure 2.

---

[*] *Corresponding author address*: Daniela Viviana Vladutescu, NYCCT/CUNY, ETET Department, Brooklyn, NY 11201. Phone 7182605300 E-mail: vvladutescu@citytech.cuny.edu

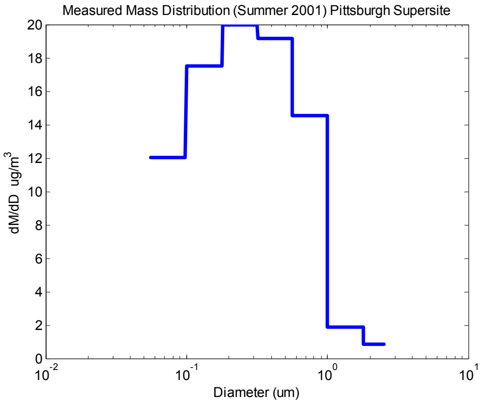

Figure 2. Number density of particles

The refractive index of the most abundant atmospheric components are given below in terms of the real and imaginary parts.

	n	k
Amon. Sulfate	1.53	0.0
Amon. Nitrate	1.55	0.0
Org.	1.81	-.25

The growth factor of particles of pure sulfate or nitrate expressed as a function of RH (relative humidity) has been developed based on empirical parametric coefficients for particular chemicals in the atmosphere given by Tang et al. (1996 and 1994). The mass equivalent growth factor of the dry solute particle is defined in Mikhailov et al., (2004) as the ratio of the droplet diameter, D_m, to the mass equivalent diameter of particle consisting of dry solute $D_{m,s}$, and is mathematically represented in formula 1.

$$g_{m,s} = \frac{D_m}{D_{m,s}} = \left(\frac{\rho_s}{x_s \rho}\right)^{1/3} \qquad (1)$$

Where x_s is the mass fraction of solute , ρ_s is the density of the dry solute and ρ the density of the mixture that can be calculated using the parametric expression below

$$\rho = \rho_w + \sum_q d_q x_s^q \qquad (2)$$

where ρ_w is the density of pure water (0.997 g/cm^3) and the polynomial coefficients are given in Tang et al. (1994) for sulfate and in Tang et al. (1996) for nitrate. For convenience these coefficients are reproduce in table 1.

Table 1

Solute	d1*10^-3	d2 *10^-6	d3*10^-8
NH_4NO_3	4.05	9	-
$(NH_4)_2SO_4$	5.92	5.036	1.024

Based on the densities of dry solutes and mixture, mass fractions and dry particle size we computed the droplet diameter D_m. This diameter in conjunction with molar mass of water, water activity and the surface tension that can be approximated as equal to the water tension ($\sigma=\sigma_w$=0.072N/m) for temperatures of 298ºF and $D_m \geq$100nm.

The water activity is calculated using the expression in formula 3

$$a_w = 1 + \sum_q c_q x_s^q \qquad (3)$$

Which is also based on empirical parameters given by the same authors mentioned above (Tang et al. 1994 and 1996) and represented in table 2

Table 2

Solute	c1 10^-3	c2 *10^-6	c3 *10^-7	c4 *10^-8
NH_4NO_3	-3.65	9.155	-2.826	-
$(NH_4)_2SO_4$	-2.715	31.13	-23.36	1.412

Using the above derived components we determined the RH(relative humidity) described by formula 4, according to Kohler theory

$$S_w = RH = a_w \exp\left(\frac{4\sigma M_w}{\rho R T D_m}\right) \qquad (4)$$

The results of pure particles growth versus RH are presented in figure 3

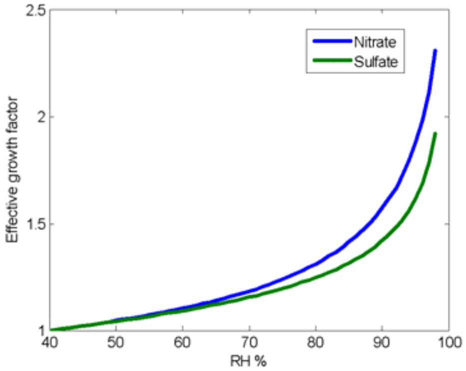

Figure 3 Calculation of growth curves

The refractive index of hygroscopic particles has been calculated based on Hanel's (1976) derivations and given here in formula 5 and 6

$$n = n_w + (n_0 + n_w)\left(g_{m,s}\right)^{-3} \qquad (5)$$

$$k = k_w + (k_0 - k_w)\left(g_{m,s}\right)^{-3} \qquad (6)$$

Where n and k are the real and respectively complex refractive index of the wet particle, n_0 and k_0 are the real and respectively imaginary refractive indexes of the dry solute and n_w and k_w

are the real and respectively imaginary refractive indexes of pure water.

The wet particles size and refractive indexes are used in the mie scattering theory to derive backscatter and extinction at different wavelengths. The backscatter expression is given in formula 7 below

$$\frac{\beta_{sca}(RH)}{\beta_{sca}(RH_0)} = \frac{\int \left[Q_{sca}\left(\frac{2\pi r}{\lambda_1}, m\right) * \left[\frac{dn}{dr}\right] * \pi r^2 \right] dr}{\int \left[Q_{sca}\left(\frac{2\pi r_0}{\lambda_1}, m_0\right) * \left[\frac{dn}{dr}\right] * \pi r_0^2 \right] dr_0} \quad (7)$$

Here, n(r) is the number density (number of particles per volume) and $\frac{dn(r)}{dr}$ is the aerosol number distribution. We note that for a given aerosol distribution, the normalized Sratio eliminates the vertical concentration effects.

The results of the backscatter and extinction for particles composed of nitrates or sulfates only are plotted versus RH in figure 3.

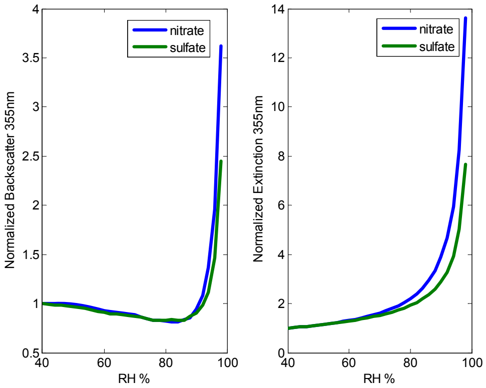

Figure 4 Backscatter and extinction for particles composed of water and nitrates or sulfates only.

As it can be noticed from figure 4 the trade off between the decrease in refractive index and growth in particle size is evident in particularly for backscatter which is consistent with the scattering theory. From analysis of the scattering function the forward scattering is insensitive to refractive index index, the total scattering almost insensitive and the backscatter is highly sensitive to it. However at higher RH (i.e after the deliquescence point which is 80-85% for sulfates) the particle size is rapidly increasing and thus it dominates the backscattering radiation, pushing the backscatter to increase. The normalized backscatter is obtained using formula 7 and is plotter in figure 5b). (A similar expression was used for the normalized extinction with the difference that the scattering efficiency was replaced by the extinction one)

The normalized backscatter and extinction to this RH of 85% are represented in figure 4a and respectively b.

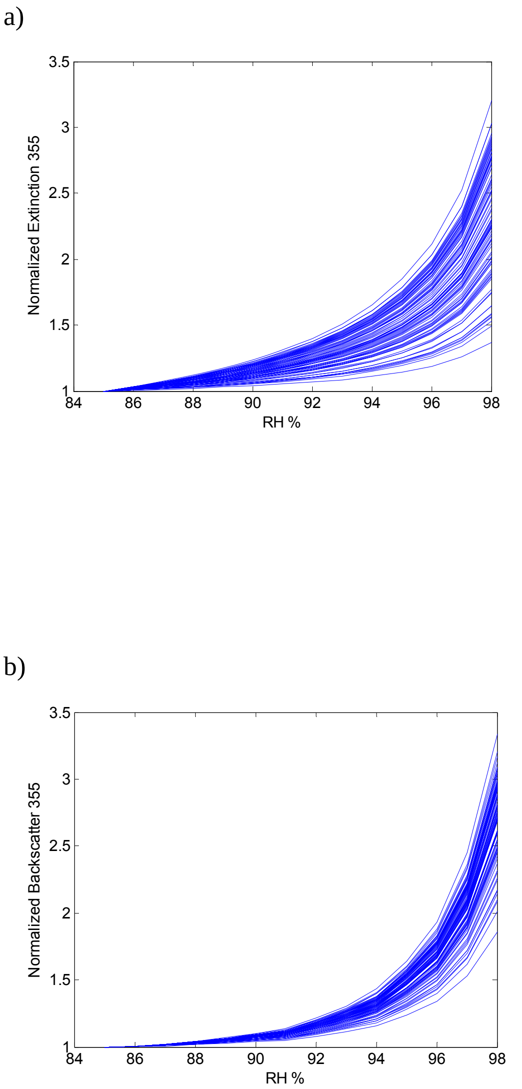

Fig. 5 a)Normalized extinction at 355nm b)normalized backscatter at 355nm with respect to extinction and respectively backscatter at 85% RH

The normalized extinction has also been analyzed versus inorganic to organic ratio and the results indicate a clear dependence of the normalized extinction at all lidar ratios of the (sulfate+nitrate)/organics ratio.

It is notable here the trend in the extinction and backscatter that can be exploited to retrieve valuable information regarding the hygroscopic properties of aerosols. However as noted from this two graphs the normalized backscatter (figure 5b) is more sensitive to variations of the number density distribution when compared to the normalized extinction (figure 5a).

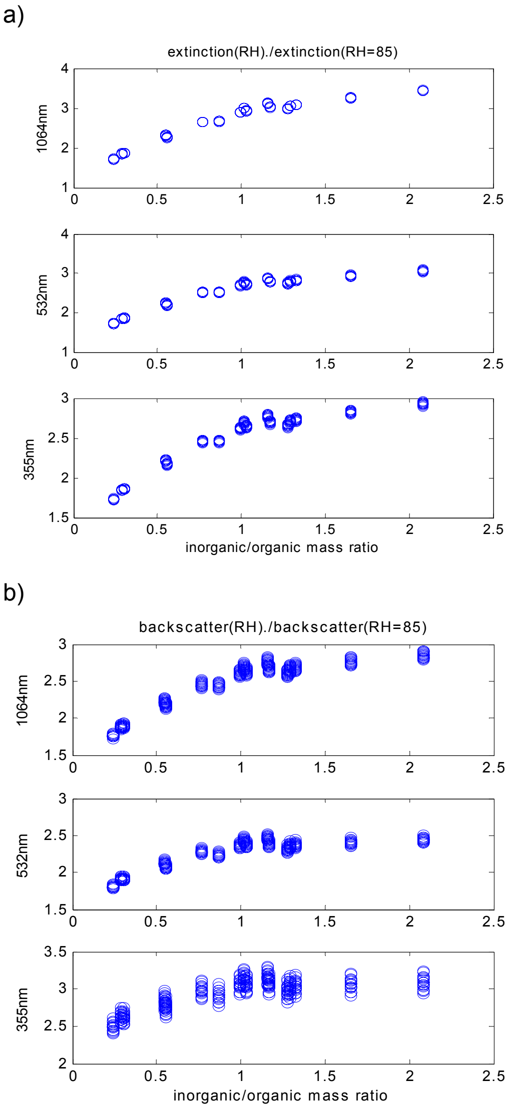

Figure 6 a, Normalized extinction and b) backscatter at 1064nm,532nm,and respectively 355nm

We are also interested in the S ratio (extinction to backscatter ratio) and we plotted the results in figure 7.

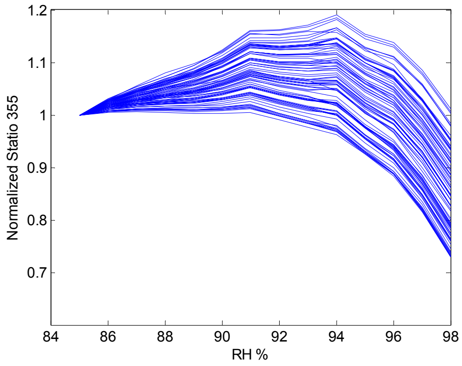

Figure 7. Normalized S ratio (355nm)

Multiple curves illustrate changes in behavior using hygroscopic and non hygroscopic component concentrations measured in summer in New York City (NYC).

Please note the downward trend in the S ratio for normalized backscatter with respect to 85%.

Color ratios are nearly constant indicating wavelength sensitivity that is negligible. The S-ratio sensitivity is also much smaller than individual extinction (or backscatter) coefficient sensitivity as indicated in figure 8b

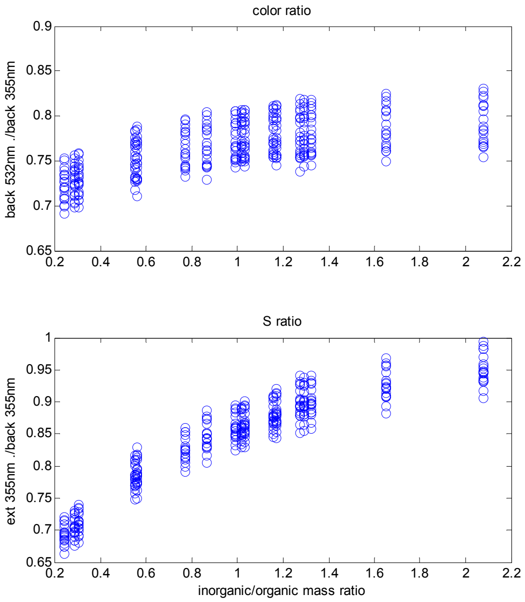

Figure 8 a) Color Ratio(532nm/355nm) and S(355nm/355nm) ratio b) Normalized S ratio at 355nm for different measured solute concentrations

3. Validation of the model with CCNY lidar measurements

3.1 CCNY Lidar system

A schematic of the CCNY lidar system is represented in fig 9

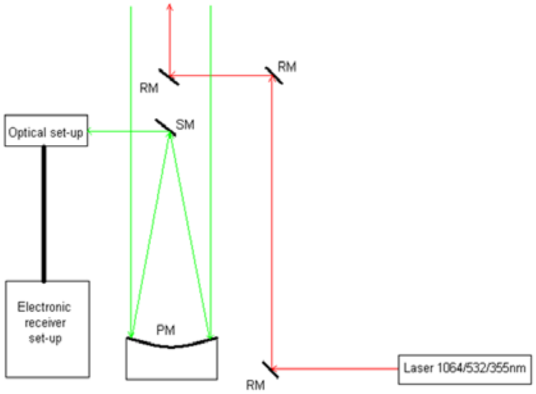

Figure 9 Schematic of the CCNY lidar system

The transmitting laser of the lidar system is a Q-switched Spectra-Physics Quanta Ray Pro230 Nd-YAG with variable output power up to 475 mJ @ 532 nm, 950 mJ @ 1064 nm and 300 mJ @ 355 nm. This system currently has five channels with wavelengths at 1064 nm, 532 nm, 355 nm, including a Raman channel at 407 nm for water with a second Raman channel at 387 for nitrogen. Repetition rate of 30 Hz with 1-2 ns pulse duration @ 532 nm; <0.5 mrad beam divergence. Beam is separated in the three components to allow power measurements on separate channels and then regrouped and directed by three dichroic mirrors into the atmosphere above the system. The beam is on the axis of the telescope. Due to the different wavelength channels, different detectors are used. An APD (silicon enhanced avalanche photodiode) for the 1064 nm (infrared) channel is used while a PMT (Hammamatsu photomultiplier tubes) is used for the 532 nm (green), 386 nm (Raman) and 355 nm (UV) and 407nm(Raman) channels. An example of lidar retrival is shown in fig 10a)

a)

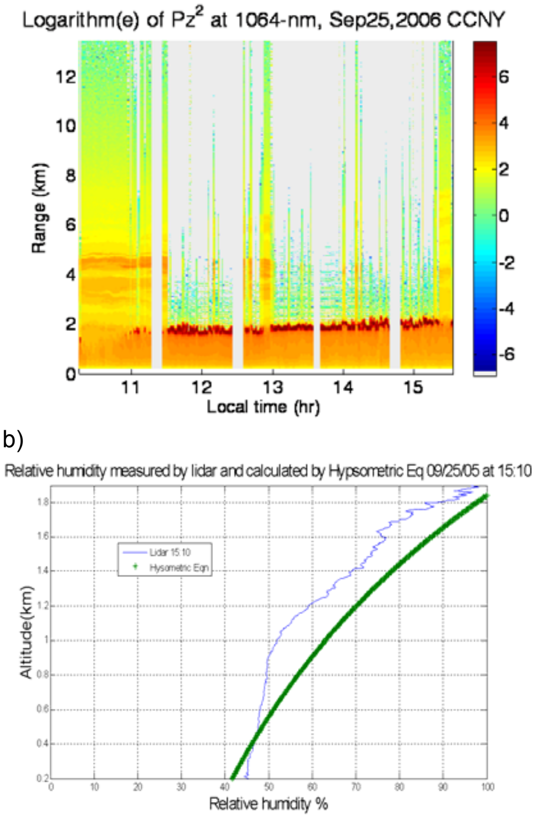

b)

Fig. 10. a)Lidar image at the 1064nm and b). Relative humidity vs. altitude on Sept 25th , 2006 at 15:10pm

The analyses of the hygroscopic properties of the aerosols have been made for the day of September 25th, 2006 due to the low cloud presence in the planetary boundary layer and the expected increase relative humidity with height. In particular, the low clouds allow us to have a fairly stable atmospheric state which can be probed vertically to high RH. The lidar image at 1064nm on September 25th, 2006 is presented in figure 10a).

The water vapor retrieval is explained in detail in Vladutescu (2007). Optimal conditions of analysis are met when well mixed boundary layers are determined. These conditions are assumed to occur under cloud capped conditions. It is important that the aerosol layer is well mixed so that changes in optical properties due to RH effects are not confused with variations in aerosol concentrations. For example, Phalow (2006) validates the well mixed condition using the hypsometric form of the ideal gas law. This approach calculates the RH for a constant mixing ratio derived from the surface alone. If the RH reaches 100 % for a height which matches the lidar derived cloud base value, we can infer well mixed conditions. To validate the well mixed conditions we simultaneously compare the predictions of the hypsometric eqn to our lidar in figure 10.

The results of the hypsometric analysis are presented in figure 9b which relates the RH to the pressure level. which agrees within 10% with the lidar determination of cloud base as seen in figure 10a.

3.2 Model validations using CCNY lidar retrievals

The following steps are describing the extinction and backscattering retrieval algorithms.

In a first stage we computed the aerosol/cloud extinction coefficient from N_2-Raman returns using the relation in formula (8):

$$\alpha_{p,c}(\lambda_0,z)=\frac{1}{1+(\frac{\lambda_N}{\lambda_0})^{-\nu}}\{\frac{d}{dz}[\ln\frac{N(z)}{P(\lambda_N,z)z^2}] \qquad (8)$$
$$-\alpha_m(\lambda_0,z)[1+(\frac{\lambda_N}{\lambda_0})^{-4}]\}$$

where N(z) is the molecular number density and the Angstrom coefficient ν=1.2 for aerosol and 0 for cloud.

The second step was to retrieve the aerosol/cloud backscatter coefficient from the N2-Raman and elastic returns. The aerosol scattering ratio R(z) from N_2-Raman and elastic returns were calculated using the relations given by equation 9:

$$R(\lambda_0,z)=\frac{\beta_p(\lambda_0,z)+\beta_m(\lambda_0,z)}{\beta_m(\lambda_0,z)}= \\ =\left[\frac{C(\lambda_N)}{C(\lambda_0)}\right]\frac{P(\lambda_0,z)}{P(\lambda_N,z)}\frac{T(\lambda_N,z)}{T(\lambda_0,z)} \tag{9}$$

where T are the transmissions at the Raman (387nm) and respectively lidar wavelength (355nm). This two transmissions can be considered equal and therefore they cancel out. With a known R(z$_{ref}$) at a reference altitude z$_{ref}$, get lidar constant ratio C and R(z):

$$R(\lambda_0,z)=\frac{P(\lambda_0,z)}{P(\lambda_N,z)}\bullet R\left(\lambda_o,z_{ref}\right) \\ \bullet\frac{P(\lambda_N,z_{ref})}{P(\lambda_0,z_{ref})}\bullet\frac{T(\lambda_N,z,z_{ref})}{T(\lambda_0,z,z_{ref})} \tag{10}$$

Finally the aerosol backscatter coefficient is calculated by plugging in the aerosol scattering ratio R(z) calculated above.

$$\beta_p(\lambda_0,z)=[R(\lambda_0,z)-1]\beta_m(\lambda_0,z) \tag{11}$$

The lidar retrieved backscatter and extinction are plotted in figure 11.

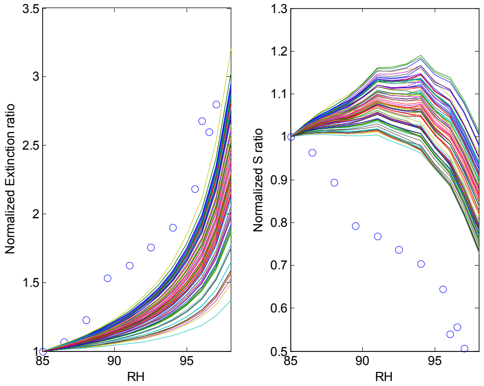

Fig 11 Aerosol normalized extinction, and S ratio at 355nm versus altitude

Lidar results are in agreement with the model indicating a decrease in the S ratio for altitudes above 1.7km where RH is higher than 85% and respectively an increase in the normalized extinction. While the normalized extinction seems to perform better there could clearly be observed a deviation of the S ratio from the model. This could be resulting from difficulties in retrieving backscatter due to far end calibration.

4. Conclusions

In the present paper we explored the possibility of determining the nature and variability of urban aerosol hygroscopic properties using multi-wavelength Raman lidar measurements at 355nm, as well as backscatter measurements at 532nm and 1064nm. The results of the model analysis taken at wavelengths 355nm and 532nm indicate a clear dependence of the backscattering and total geometric cross section on relative humidity and in particular both normalized extinction and backscatter at 355nm modifications in the RH range from 85-98% are clearly sensitive to hygroscopic growth.

However, normalized backscatter coefficients alone are more sensitive to changes in underlying number distributions. Both S–ratios and color ratios have the advantage of being insensitive to number density changes but normalized color ratios are also insensitive to hygroscopic growth effects.

Comparison of theoretical scattering growth curves with measurements are in qualitative agreement which is the best that can be expected with the approximations made. More mathematical investigations of the new proposed analyses should be performed on the lidar data to determine the degree of agreement of the measurements to the theoretical models based on the different models inputs. In addition, some qualitative features of the hygroscopic properties is demonstrated from lidar measurements under low cloud conditions.

Further efforts are needed to update the aerosol hygroscopic model and this approach will be further refined during the Summer 2009 measurement campaign at Queens College.

An updated model database together with backward trajectory analysis is needed to develop a suitable climatology of hygroscopic aerosols. Further validation using hourly insitu measurements will be implemented to allow retrieval validations at a high temporal resolution. Ground based multiwavelength nephelometer, TSI SMPS (Scanning Mobility Particle Sizer spectrometers) for size distribution, TEOM (Tapered Element Oscillating Microbalance) for mass of particles and Aeronet (NOAA ARL) refractive indexes analyses will also be explored.

5. *References*

R.A. Ferrare, 1998: Raman lidar measurements of aerosol extinction and backscattering 2. Derivation of aersol refractive index, single scattering albedo, and humidification factor using Raman lidar and aircraft size distribution measurements, *J. of Geophy. Res.*,103, 19673-19689

Cabada J.C., 2004: Light scattering by fine particles during the Pittsburgh Air Quality Study: Measurements and modeling, *J. of Geophy. Res.*,109, D16S03

Hanel G., 1976: The properties of Atmospheric aerosol particles as functions of the relative humidity at thermodynamic equilibrium with the surrounding moist air, *Adv. Geophy*., 19, 73-188

Mikhailov E., 2004: Interaction of aerosol particles composed of protein and salts with water vapor: hygroscopic growth and microstructural rearrangement, *Atmos. Chem. Phys.*, 4, 323-350

Phalow M., 2006: Comparison between lidar and nephelometer measurements of aerosol hygroscopicity at Southern Great Plains Atmospheric Radiation Measurement site, *J. of Geophy. Res*.,111, DO5S15

Tang I.N., 1996: Chemical and size effects of hygroscopic aerosols on light scattering coeffiecients, *J. of Geophy. Res*.,101, 19245-19250

Tang I.N., 1994: Chemical and size effects of hygroscopic aerosols on light scattering coeffiecients, *J. of Geophy. Res*.,99, 18801-18808

Vladutescu D. V., 2007: Analyses of Raman lidar calibration techniques based on water vapor mixing ratio measurements, *WSEAS Trans. on Syst*., 2, 4, 651–658,